SUPPORTING INFORMATION

Understanding the Catalytic Site Structure in Metal Poly(Heptazine Imide) – Crystalline Carbon Nitride

Dario Calvani,[1,2,] Isadora G. Farias,[3] Diandra Nunes Barreto,[3] Luis F. G. Noleto,[3] Marcos A. R. da Silva,[3] Ivo F. Teixeira,[3,*] Agnieszka Kuc,[1,2,*] Thomas D. Kühne.[1,2]*

1. Helmholtz-Zentrum Dresden-Rossendorf (HZDR), Bautzner Landstrasse 400, 01328 Dresden, Germany.

2. Center for Advanced Systems Understanding (CASUS), Conrad-Schiedt-Strasse 20, 02826 Görlitz, Germany.

3. Department of Chemistry, Federal University of São Carlos, 13565-905, São Carlos, SP, Brazil.

* To whom correspondence should be addressed: d.calvani@hzdr.de, ivo@ufscar.br, a.kuc@hzdr.de.

S1. Characterization of Ni-PHI

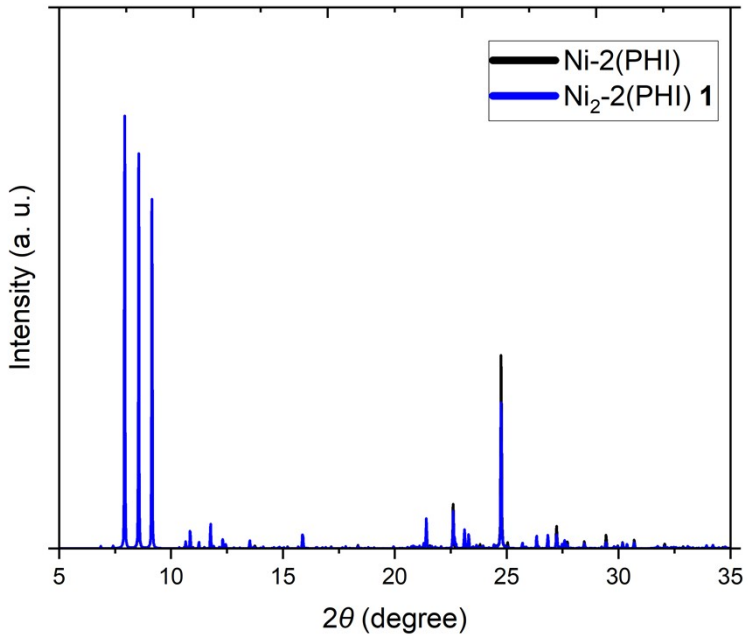

Figure S1. X-ray diffraction (XRD) patterns extracted from the DFT+*U* geometry optimizations (detailed in the DFT-based static simulations section) of Ni-2(PHI) and Ni_2-2(PHI) system **1**, in black and blue lines, respectively, using λ = 1.5418 Å.

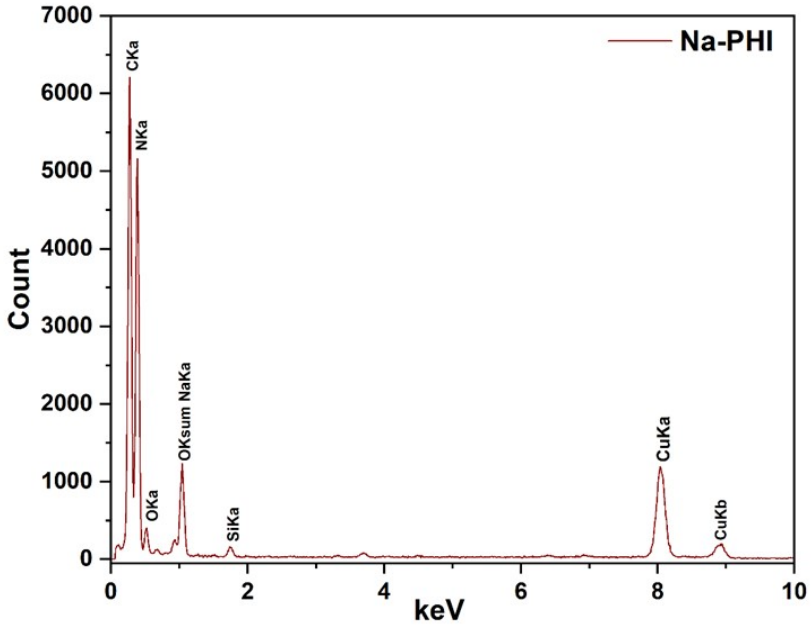

Figure S2. EDS spectrum of the Na-PHI sample.

Table S1. The quantification of nickel loading was performed by inductively coupled plasma optical emission spectroscopy (ICP-OES) using a Thermo iCAP 6500 instrument.

Material	Fraction (wt%)
Ni-PHI 0.5 wt%	**0.56**
Ni-PHI 1 wt%	**1.06**
Ni-PHI 2 wt%	**2.34**
Ni-PHI 4 wt%	**4.72**

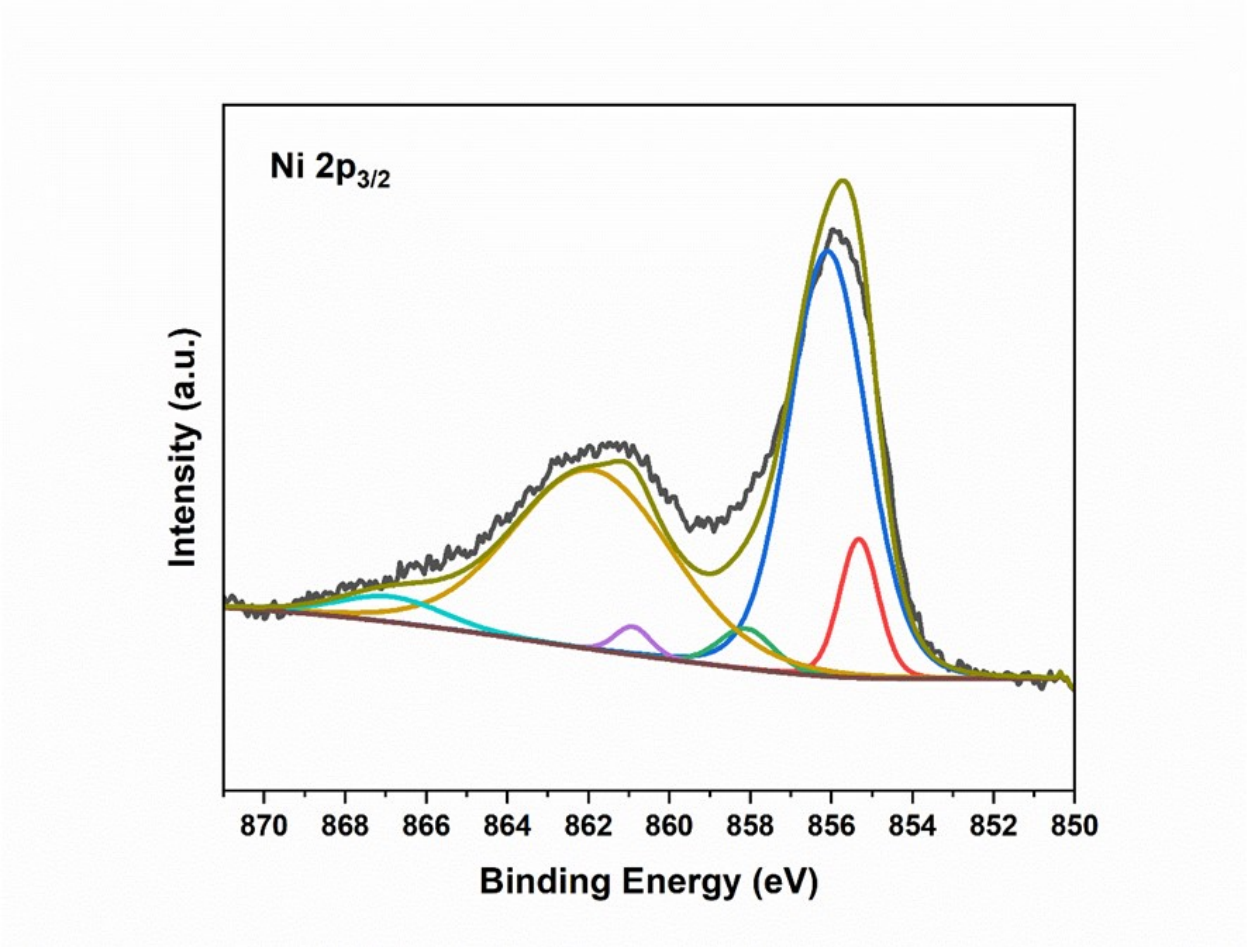

Figure S3: Representative peak fitting of the Ni 2p XPS region for Ni-PHI 4 wt%. The deconvoluted components are modeled based on $Ni(OH)_2$ standard parameters to identify the nickel oxidation state.

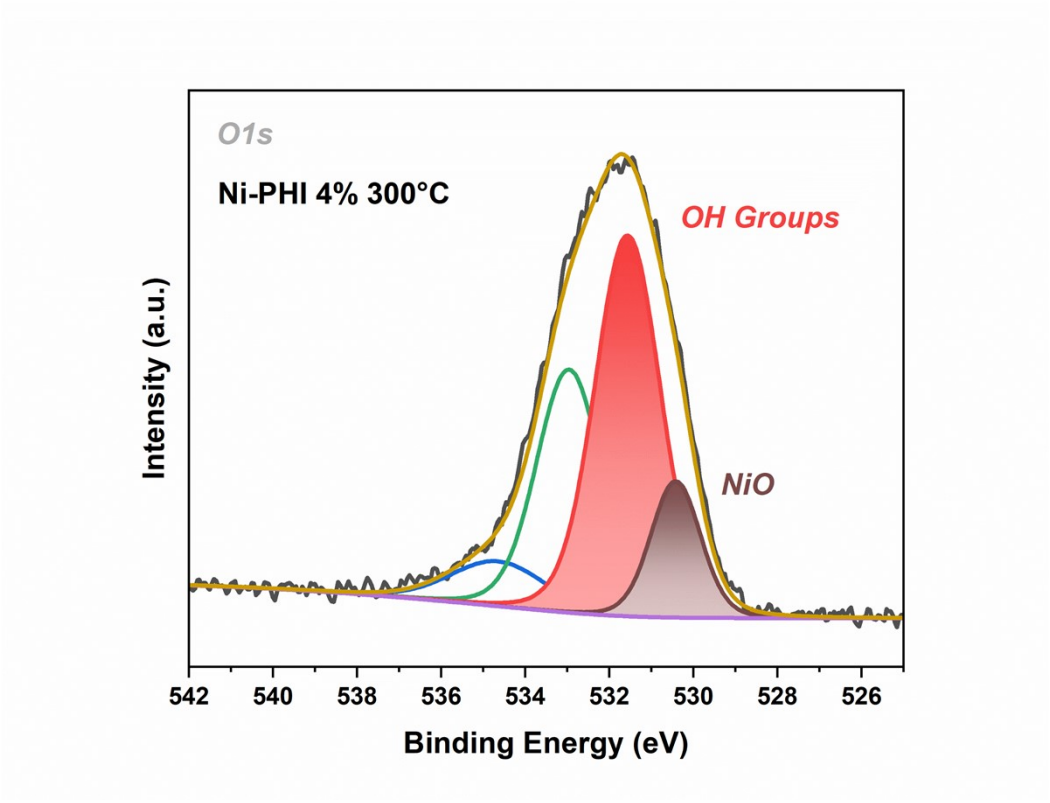

Figure S4: High-resolution O1s XPS of Ni-PHI 4% after thermal treatment.

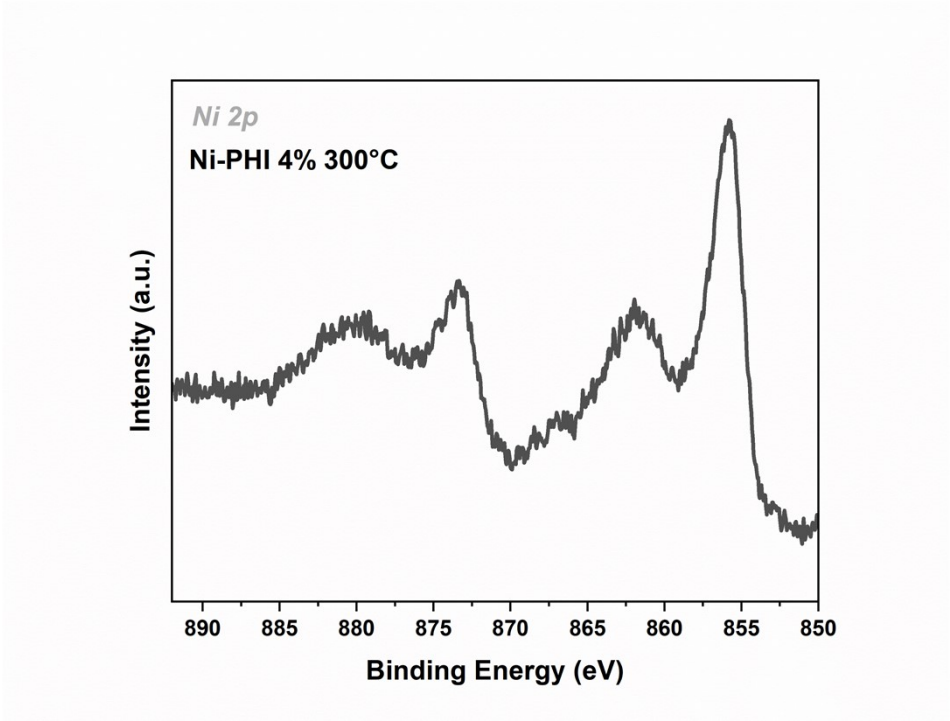

Figure S5: High-resolution O1s XPS of Ni-PHI 4% after thermal treatment.

S2. Computational Results on Ni_{1or2}-2(PHI) and (Ni_{1or2}-CO)-2(PHI): DFT-based Static Simulations

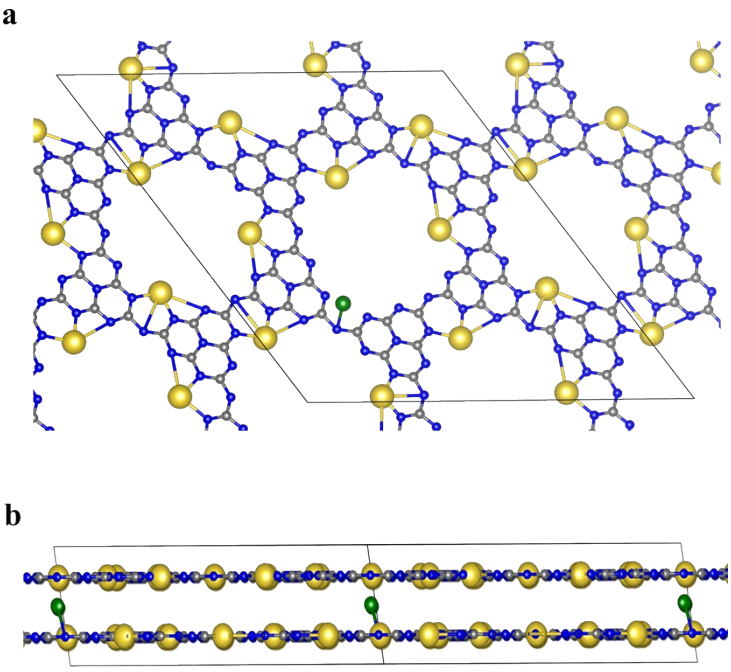

Figure S6. **a**, Top, and **b**, side views, respectively, before geometry optimization of the 2(PHI) layers with out-of-plane Ni^{2+} ion: Ni-2(PHI), with the simulation box in black solid line. The atoms are depicted as ball-and-stick models, with nickel in green, carbon in grey, nitrogen in blue, and sodium in yellow.

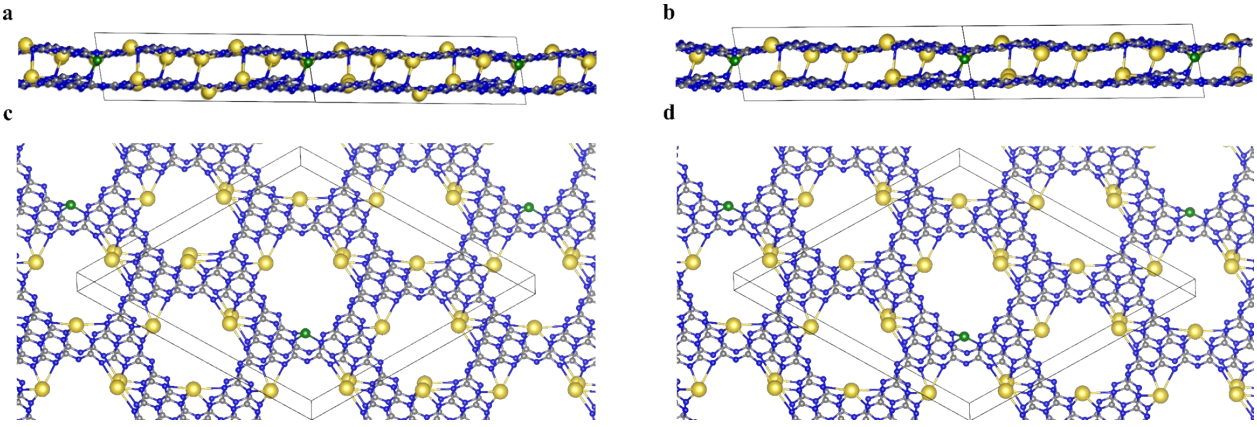

Figure S7. Side and top views DFT+*U* geometry-optimized configurations 2(PHI) layers from starting configurations in **a**,**c**, out-of-plane, and **b**,**d**, in-plane, Ni^{2+} ion: Ni-2(PHI). The atoms are depicted as ball-and-stick models, with nickel in green, carbon in grey, nitrogen in blue, and sodium in yellow.

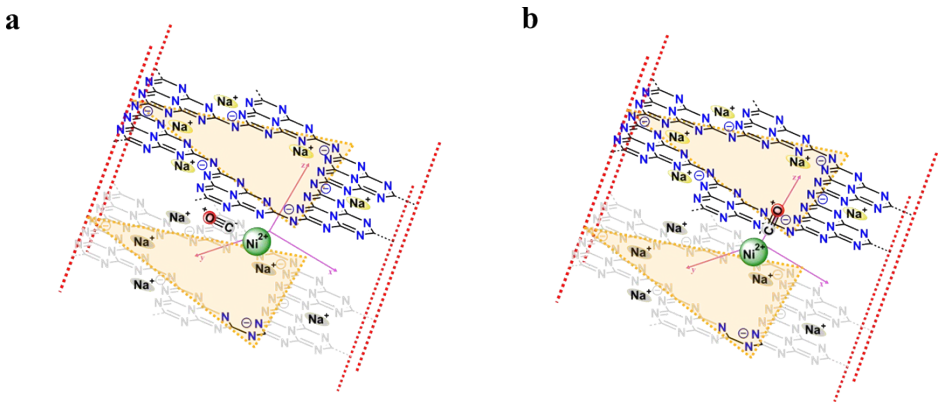

Figure S8. Idealized (Ni-CO)-2(PHI) system with an out-of-plane Ni^{2+} ion and interacting CO molecular probe placed in two starting positions: along **a**, the z-axis, and **b**, the x-y plane passing through the Ni^{2+} ion, respectively. The orange area describes the catalytically active site with the Ni^{2+} ion. The atoms are sketched in ball-and-stick representation, with nickel in green, carbon in black, nitrogen in blue, oxygen in red, and sodium in yellow. In color and grey, the upper and bottom, respectively, are PHI layers and sodium cations. The interacting part of the bottom PHI layer with the Ni^{2+} ion is kept colored. The reference x, y, and z axes to mark the initial CO orientation are shown in pink.

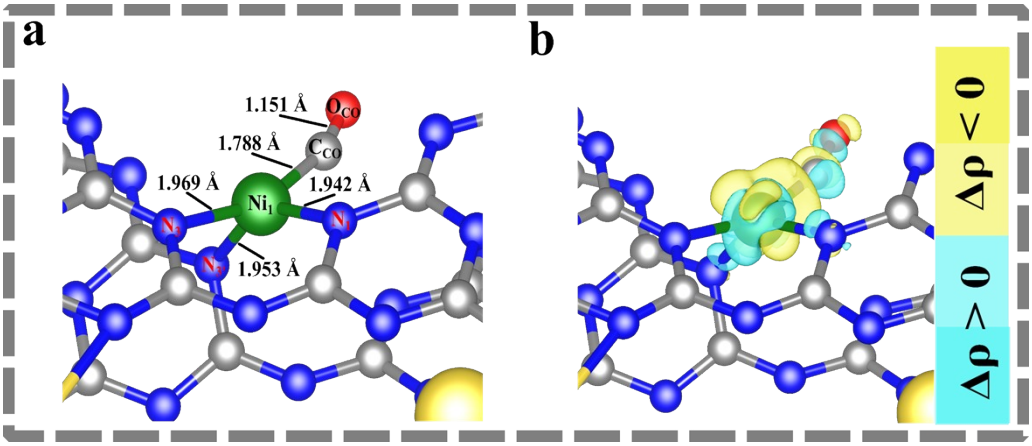

Figure S9. a, Zoom on the DFT geometry optimized (Ni-CO)-2(PHI) system to highlight the Ni_1-C_{CO}, C_{CO}-O_{CO}, and Ni-N_n (Ni_1-N_1, Ni_1-N_3, and Ni_1-$N_{3'}$) distances. **c**, DFT charge density difference ($\Delta\rho$) for the (Ni-CO)-2(PHI) system. Yellow and cyan colors are used to represent the negative and positive charge density differences, respectively, with an isosurface value of 0.01. The atoms are depicted as ball-and-stick models, with nickel in green, carbon in grey, nitrogen in blue, oxygen in red, and sodium in yellow.

Table S2. DFT+*U* Bader charge for Ni_{1or2}, C_{CO}, and O_{CO}, in Ni-2(PHI), and (Ni-CO)-2(PHI) systems, and (Ni_2)-2(PHI) and (Ni_2-CO)-2(PHI) systems **1**, **2** and **3**.

System	**Ni_1 Bader charge**	**Ni_2 Bader charge**	**C_{CO} Bader charge**	**O_{CO} Bader charge**
Ni-2(PHI)	+1.11 |*e*|	-	-	-
(Ni-CO)-2(PHI)	+0.96 |*e*|	-	+1.84 |*e*|	−1.80 |*e*|
(Ni_2)-2(PHI) system **1**	+0.88 |*e*|	+0.81 |*e*|	-	-
(Ni_2-CO)-2(PHI) system **1**	+0.92 |*e*|	+0.84 |*e*|	+1.71 |*e*|	−1.80 |*e*|
(Ni_2)-2(PHI) system **2**	+1.16 |*e*|	+1.13 |*e*|	-	-
(Ni_2-CO)-2(PHI) system **2**	+1.14 |*e*|	+1.12 |*e*|	+1.83 |*e*|	−1.78 |*e*|
(Ni_2)-2(PHI) system **3**	+1.14 |*e*|	+1.11 |*e*|	-	-
(Ni_2-CO)-2(PHI) system **3**	+1.09 |*e*|	+1.14 |*e*|	+1.82 |*e*|	−1.79 |*e*|

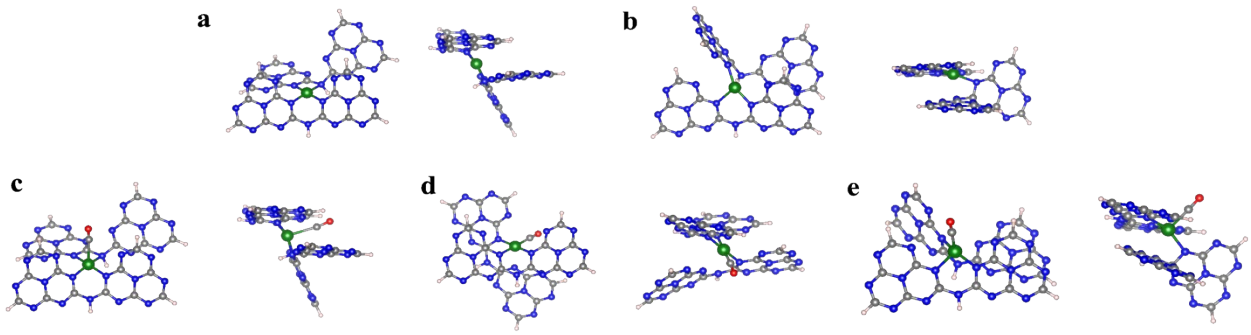

Figure S10. DFT (PBE0-D3) optimized geometries: **a**, $[Ni\text{-}(melem)_2]^{2+}$singlet spin state, **b**, $[Ni\text{-}(melem)_2]^{2+}$triplet spin state, **c**, $[(Ni\text{-}CO)\text{-}(melem)_2]^{2+}$ singlet spin state from singlet spin state $[Ni\text{-}(melem)_2]^{2+}$optimized geometry, **d**, $[(Ni\text{-}CO)\text{-}(melem)_2]^{2+}$ singlet spin state from triplet spin state $[Ni\text{-}(melem)_2]^{2+}$ optimized geometry, **e**, $[(Ni\text{-}CO)\text{-}(melem)_2]^{2+}$ triplet spin state from triplet spin state $[Ni\text{-}(melem)_2]^{2+}$optimized geometry.

Table S3. DFT (PBE0-D3) geometry optimization results: Energy (E) in eV, distances (d) in Å, and the Bader charge on Ni, of $[Ni\text{-}(melem)_2]^{2+}$ and $[(Ni\text{-}CO)\text{-}(melem)_2]^{2+}$ complexes. Reported distances include $<Ni\text{-}N_n>$ (averaged value), where N_n denotes the four nitrogen atoms closest to Ni, as well as $Ni\text{-}C_{CO}$, and $C_{CO}\text{-}O_{CO}$. The free CO stretching frequency is found to be equal to 2235.87 cm^{-1}, in agreement with previous literature at the same calculation level.[1]

System	E (eV)	$<d(Ni\text{-}N_n)>$ (Å)	$d(Ni\text{-}C_{CO})$ (Å)	$d(C_{CO}\text{-}O_{CO})$ (Å)	Ni Bader Charge
$[Ni\text{-}(melem)_2]^{2+}$ singlet spin state	−110695.1392	1.907	-	-	+1.23 $\|e\|$
$[Ni\text{-}(melem)_2]^{2+}$ triplet spin state	−110695.5599	2.030	-	-	+1.32 $\|e\|$
$[(Ni\text{-}CO)\text{-}(melem)_2]^{2+}$ singlet spin state from singlet spin state $[Ni\text{-}(melem)_2]^{2+}$ optimized geometry	−113775.4629	1.927	2.414	1.131	+0.99 $\|e\|$
$[(Ni\text{-}CO)\text{-}(melem)_2]^{2+}$ singlet spin state from triplet spin state $[Ni\text{-}(melem)_2]^{2+}$ optimized geometry	−113776.7907	2.095	1.853	1.130	+1.11 $\|e\|$
$[(Ni\text{-}CO)\text{-}(melem)_2]^{2+}$ triplet spin state from triplet spin state $[Ni\text{-}(melem)_2]^{2+}$ optimized geometry	−113776.513	2.041	2.030	1.125	+1.20 $\|e\|$
Free CO	−3080.00	-	-	1.134	-

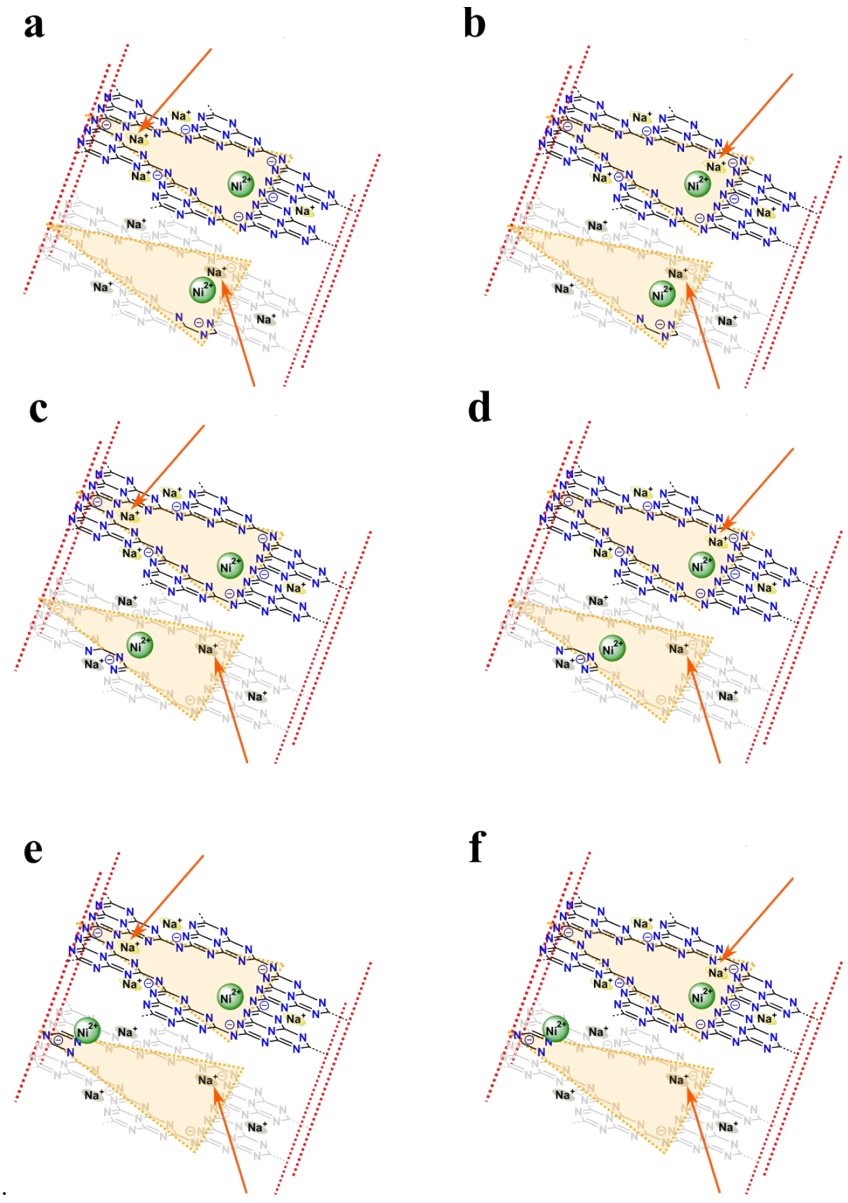

Figure S11. Idealized 2PHI layers with three and two permutated starting positions of the out-of-plane Ni^{2+} ions, and the Na^{+} ions in the catalytic pocket, respectively: Ni_2-2(PHI). The orange area describes the catalytically active site with Ni^{2+} ions. The atoms are depicted as ball-and-stick models, with nickel in green, carbon in black, nitrogen in blue, and sodium in yellow. In color and grey, the upper and bottom, respectively, are PHI layers and sodium cations. The starting interacting part of the bottom PHI layer with the Ni^{2+} ions is kept colored. The two Na^{+} ions in the catalytic site were considered in two possible swapped arrangements (orange arrows) with respect to each pair of Ni^{2+} ion position in the catalytic pocket, **a**, **b**, (top) **c**, **d**, (middle), and **e**, **f**, (bottom), respectively, resulting in a total of six configurations.

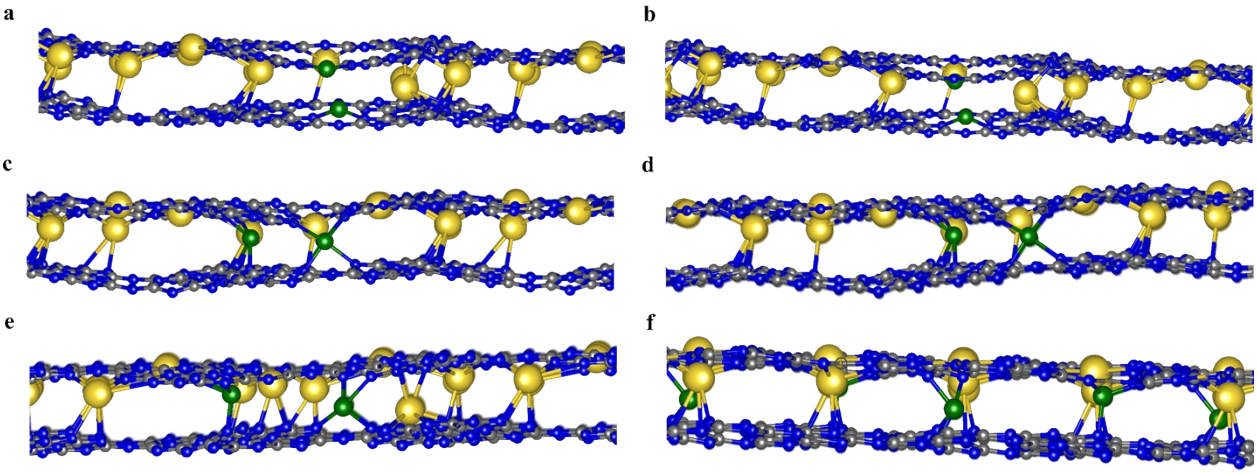

Figure S12. **a**, **c**, and **e**, DFT+*U*, and **b**, **d**, and **f**, DFT, most stable geometry-optimized configurations of 2PHI layers with out-of-plane two Ni^{2+} ions: Ni_2-2(PHI). The atoms are depicted as ball-and-stick models, with nickel in green, carbon in grey, nitrogen in blue, and sodium in yellow.

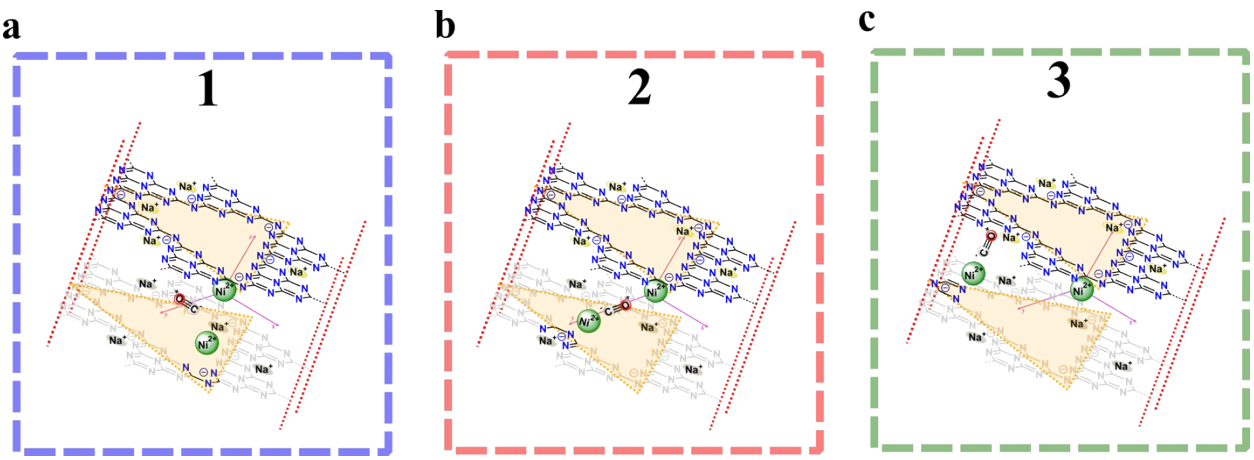

Figure S13. DFT case: representative initial idealized three configurations of two out-of-plane Ni^{2+} ions within 2PHI layers with adsorbed carbon monoxide molecular probe, (Ni_2-CO)-2(PHI): **a**, (system **1**), **b**, (system **2**), and **c**, (system **3**), respectively. The orange area describes the catalytically active site with Ni^{2+} ions. The atoms are depicted as ball-and-stick models, with nickel in green, carbon in black, nitrogen in blue, oxygen in red, and sodium in yellow. In color and grey, the upper and bottom, respectively, are PHI layers and sodium cations. The interacting part of the bottom PHI layer with the Ni^{2+} ion is kept colored. The reference *x*, *y*, and *z* axes to mark the initial CO orientation are shown in pink.

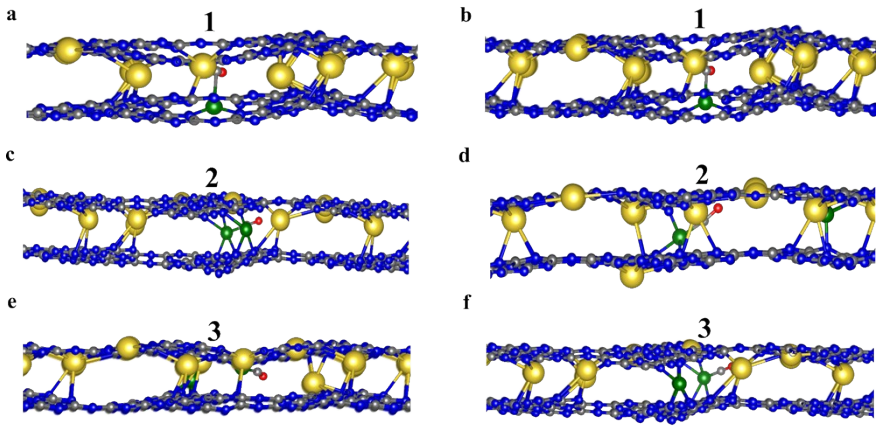

Figure S14. Side views of **a**, **c**, and **e**, DFT+*U*, and **b**, **d**, and **f**, DFT, most stable geometry-optimized configurations of 2PHI layers with carbon monoxide molecular probe, (Ni_2-CO)-2(PHI), system **1**, system **2**, and system **3**, respectively. The atoms are depicted as ball-and-stick models, with nickel in green, carbon in grey, nitrogen in blue, oxygen in red, and sodium in yellow.

Table S4. DFT (PBE-D3) results: binding energy (ΔE_B) in eV of $Ni_{1,2}$-CO interaction, $<Ni_{1,2}\text{-}N_n>$ (averaged value), $Ni_{1,2}$-C_{CO}, and C_{CO}-O_{CO} distances (d) in Å for the systems (Ni_2-CO)-2(PHI), **1**, **2**, and **3**, respectively, with N_n atoms ($1 \geq n \geq 18$), without and with the single quote symbol (') for the top and the bottom PHI layers (Figure 5 a), respectively. The binding energy is calculated as $\Delta E_B = E_{(Ni_2\text{-CO})\text{-2PHI}} - E_{Ni_2\text{-2(PHI)}} - E_{CO}$, where the right energy parameters are extracted from single-point calculations on (Ni_2-CO)-2(PHI), and their components Ni_2-2(PHI) and CO, respectively.

System	**ΔE_B (eV)**	**$<d(Ni_n\text{-}N_n)>$ (Å)**	**$d(Ni_n\text{-}C_{CO})$ (Å)**	**$d(C_{CO}\text{-}O_{CO})$ (Å)**
(Ni_2-CO)-2(PHI) system **1**	−2.05	1.951 (Ni_1) 1.905 (Ni_2)	1.824 (Ni_1) 2.135 (Ni_2)	1.161
(Ni_2-CO)-2(PHI) system **2**	−1.60	2.015 (Ni_1) 2.085 (Ni_2)	1.820 (Ni_2)	1.148
(Ni_2-CO)-2(PHI) system **3**	−1.95	1.943 (Ni_1) 1.925 (Ni_2)	1.780 (Ni_2)	1.148

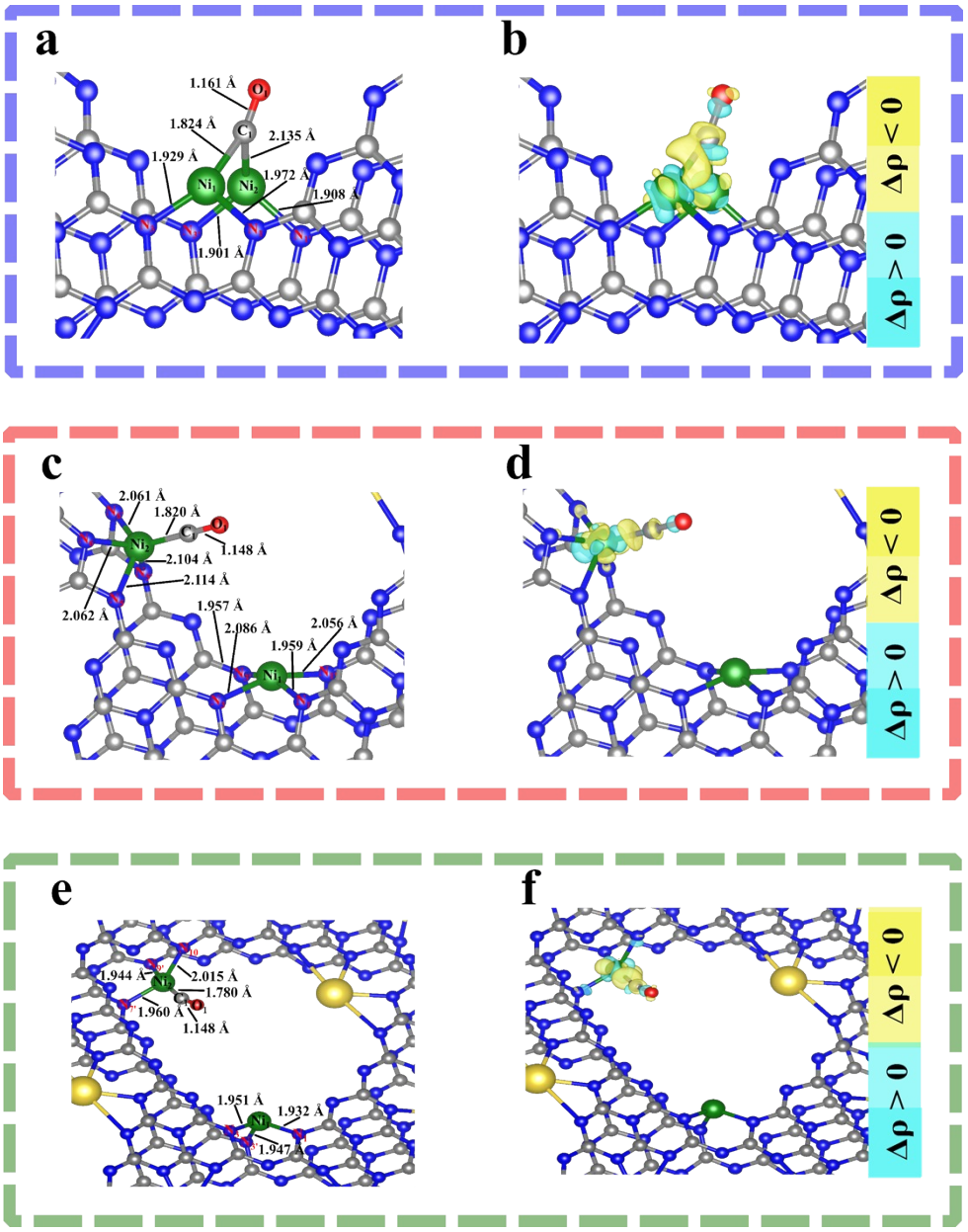

Figure S15. DFT geometry-optimized three configurations of two out-of-plane Ni^{2+} ions within PHI layers with adsorbed carbon monoxide molecular probe, (Ni_2-CO)-2(PHI): **a**, (system **1**), **c**, (system **2**), and **e**, (system **3**), inside the blue, red, and green dashed line boxes, respectively. Highlighted $Ni_{1,2}$-C_{CO}, C_{CO}-O_{CO}, and $Ni_{1,2}$-N_n distances, with N_n atoms ($1 \geq n \geq 18$), without and with the single quote symbol (') for the top and the bottom PHI layers, respectively. DFT charge density difference (Δρ) for the (Ni_2-CO)-2(PHI) system: **b**, (system **1**), **d**, (system **2**), and **f**, (system **3**), inside the blue, red, and green dashed line boxes, respectively. Yellow and cyan colors are employed for the negative and positive charge density difference, respectively, and the isosurface value = 0.01. The atoms are depicted as ball-and-stick models, with nickel in green, carbon in grey, nitrogen in blue, oxygen in red, and sodium in yellow.

S3. Computational Results on a NiO/$Ni(OH)_2$-Nanoparticle Representative Models: DFT-based Static Simulations

Table S5. DFT+*U* Bader charges for Ni_n, O_n, C_{CO}, and O_{CO} in ($Ni_{10}O_8$)-2(PHI), and ($Ni_{10}O_8$-CO)-2(PHI) systems. Ni_2 and Ni_5 are reported in bold since they are the atoms interacting with the CO molecular probe.

System/Bader charges	($Ni_{10}O_8$)-2(PHI)	($Ni_{10}O_8$-CO)-2(PHI)
Ni_1 Bader charge	+1.10 |*e*|	+1.19 |*e*|
Ni_2 Bader charge	**+0.69 |*e*|**	**+0.92 |*e*|**
Ni_3 Bader charge	+0.83 |*e*|	+0.86 |*e*|
Ni_4 Bader charge	+1.11 |*e*|	+1.11 |*e*|
Ni_5 Bader charge	**+1.07 |*e*|**	**+1.06 |*e*|**
Ni_6 Bader charge	+0.89 |*e*|	+0.88 |*e*|
Ni_7 Bader charge	+1.08 |*e*|	+1.08 |*e*|
Ni_8 Bader charge	+1.13 |*e*|	+1.13 |*e*|
Ni_9 Bader charge	+1.19 |*e*|	+1.20 |*e*|
Ni_{10} Bader charge	+1.20 |*e*|	+1.19 |*e*|
O_1 Bader charge	− 1.08 |*e*|	− 1.13 |*e*|
O_2 Bader charge	− 1.11 |*e*|	− 1.10 |*e*|
O_3 Bader charge	− 1.12 |*e*|	− 1.07 |*e*|
O_4 Bader charge	− 1.06 |*e*|	− 1.13 |*e*|
O_5 Bader charge	− 1.11 |*e*|	− 1.11 |*e*|
O_6 Bader charge	− 1.11 |*e*|	− 1.16 |*e*|
O_7 Bader charge	− 1.18 |*e*|	− 0.64 |*e*|
O_8 Bader charge	− 0.64 |*e*|	− 1.10 |*e*|
Sum of the Bader charges for the NiO	**+1.91 |*e*|**	**+2.14 |*e*|**
C_{CO} Bader charge	-	+ 1.45 |*e*|
O_{CO} Bader charge	-	− 1.84 |*e*|

To address the possible residual presence of $Ni(OH)_2$ nanoparticles, we produced a representative $(Ni_9(OH)_{14})$-2(PHI) model, selected to have the stable hexagonal β-phase $Ni(OH)_2$ crystal structure, fitting the PHI pore volume,[2] and providing a site for CO probe interaction. The total net charge of the entire system in our 2D periodic framework was set equal to zero by removing four of the six Na^+ ions from an ideal Na-saturated PHI active site, thus describing a charged $(Ni_9(OH)_{14})^{4+}$ cluster. The configuration of $(Ni_9(OH)_{14})^{4+}$ is chosen so that the distances between the nickel and OH groups at the edges of the simulation box are consistent with a periodic $Ni(OH)_2$ cluster under periodic boundary conditions (PBC). First, we performed a DFT+*U* geometry optimization of the $(Ni_9(OH)_{14})$-2(PHI) system (Figure 16 a, and c top). Then, on the optimized $(Ni_9(OH)_{14})$-2(PHI) system, we added a CO molecular probe in the vicinity of two nickel atoms $d(Ni_n\text{-}C_{CO}) \approx 2$ Å, and performed another DFT+*U* geometry optimization on the $(Ni_9(OH)_{14}$-CO)-2(PHI) (Figure 9 b, c bottom, and d). The protocol used for the DFT-based static calculations follows the Computational Methods section. The CO bond elongates to 1.156 Å when interacting with only one Ni atom of the $Ni(OH)_2$ cluster (Figure 16 b). The $Ni_1\text{-}C_{CO}$ and $Ni_2\text{-}C_{CO}$ bond lengths are 1.785 Å and 3.732 Å, respectively (Figure 16 b). The charge density difference analysis (Figure 16d) shows localization of both positive and negative isosurfaces on the O_{CO}, along with a negative isosurface on the C_{CO} atoms. The sum of the Bader charges indicates that CO is less negatively charged (−0.15 $|e|$) compared to CO in $(Ni_{10}O_8$-CO)-2(PHI) where it carries a charge of −0.39 $|e|$. The binding energy (ΔE_B) of approximately 1.60 eV is similar to that for $(Ni_{10}O_8$-CO)-2(PHI). Overall, these findings suggest a preferential Ni-CO interaction over a semi-bridge or bridge one with a small π-backdonation from the Ni atom that binds with the CO molecular probe.

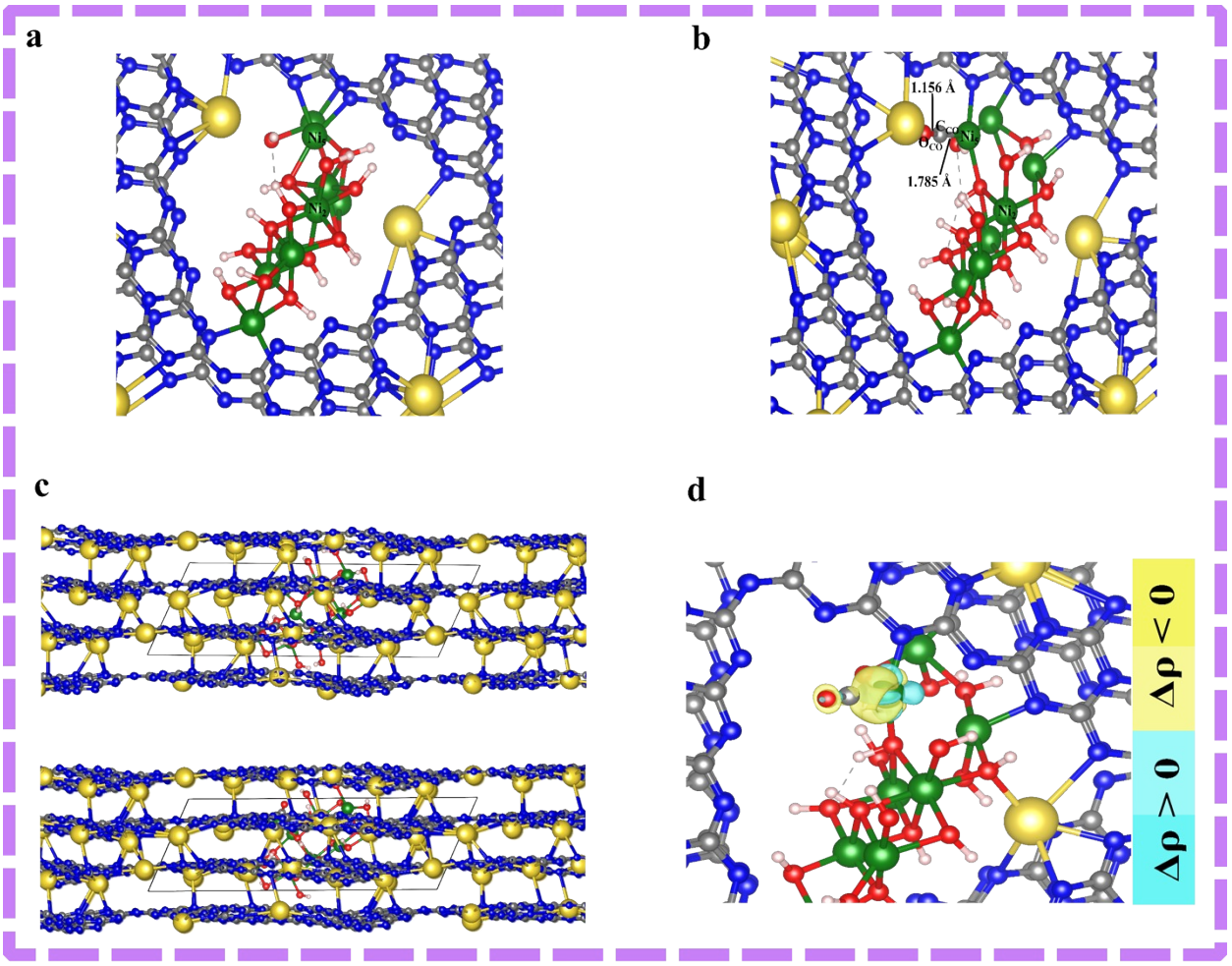

Figure S16. DFT+*U* geometry-optimized configurations of **a**, $(Ni_9(OH)_{14})$-2(PHI), **b**, $(Ni_9(OH)_{14}$-CO)-2(PHI), respectively. Highlighted $Ni_{1,2}$-C_{CO}, and C_{CO}-O_{CO}. **c**, Side views of DFT+*U* geometry-optimized $(Ni_9(OH)_{14})$-2(PHI), and $(Ni_9(OH)_{14}$-CO)-2(PHI) systems, top and bottom, respectively. **d**, DFT+*U* charge density difference ($\Delta\rho$) for the $(Ni_9(OH)_{14}$-CO)-2(PHI) system. Yellow and cyan colors are used to represent the negative and positive charge density differences, respectively, with an isosurface value of 0.01. The atoms are depicted as ball-and-stick models, with nickel in green, carbon in grey, nitrogen in blue, oxygen in red, hydrogen in white, and sodium in yellow.

S4. Computational Results: DFT-based Molecular Dynamics Simulations

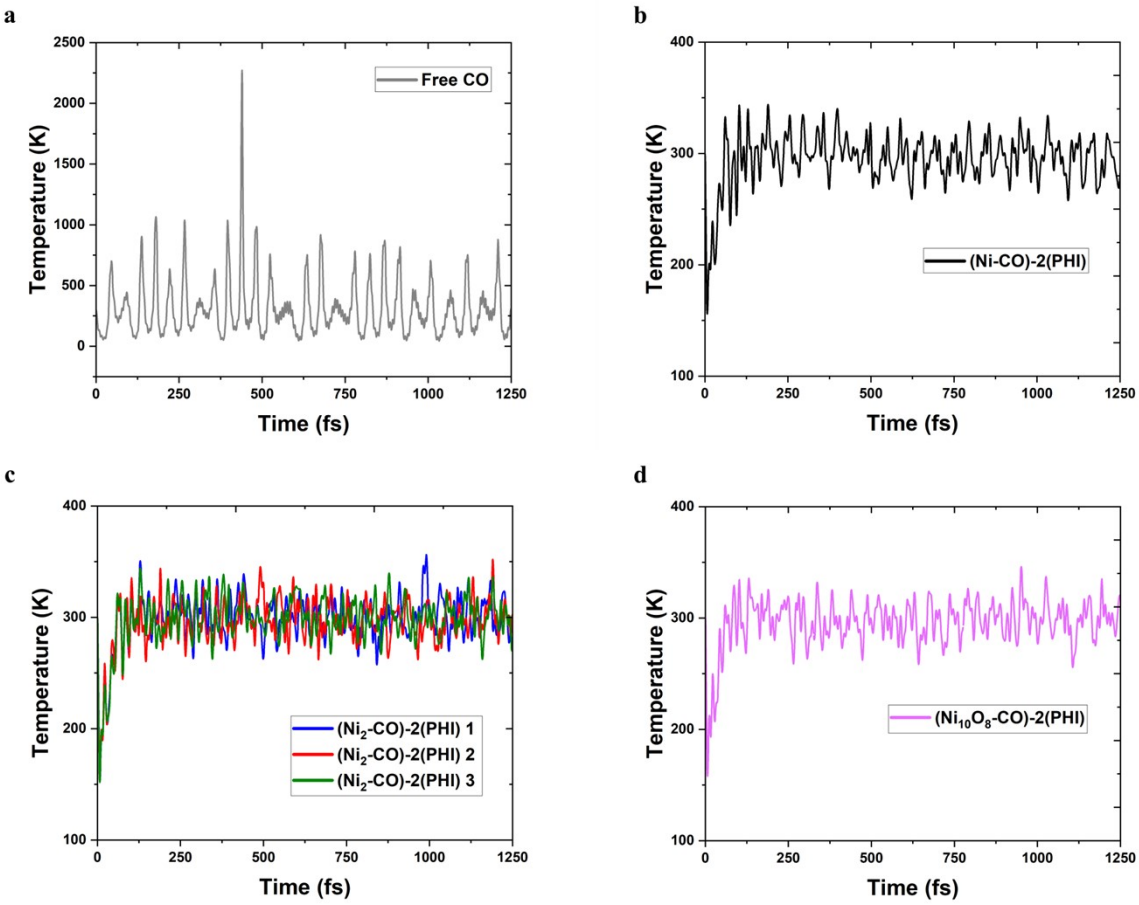

Figure S17. Time evolution of the temperature (K) along 1.25 ps of each NVT DFT-MD equilibration for **a**, the free CO in grey line, **b**, the (Ni-CO)-2(PHI) system in black line, **c**, (Ni_2-CO)-2(PHI) systems **1**, **2**, and **3**, in blue, red, and green lines, respectively, and **d**, ($Ni_{10}O_8$-CO)-2(PHI) system in pink line.

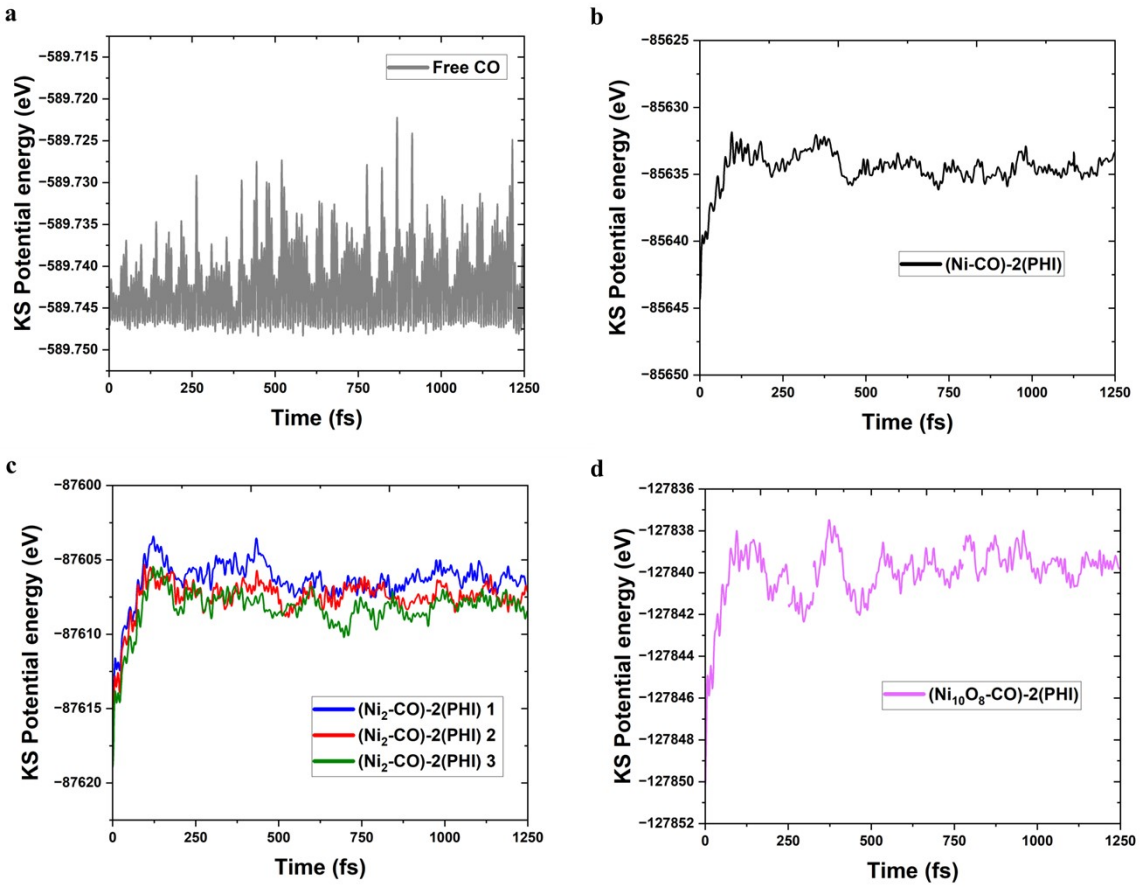

Figure S18. Time evolution of the KS potential energy along 1.25 ps of each NVT DFT-MD equilibration for **a**, the free CO in grey line, **b**, the (Ni-CO)-2(PHI) system in black line, **c**, (Ni_2-CO)-2(PHI) systems **1**, **2**, and **3**, in blue, red, and green lines, respectively, and **d**, ($Ni_{10}O_8$-CO)-2(PHI) system in pink line.

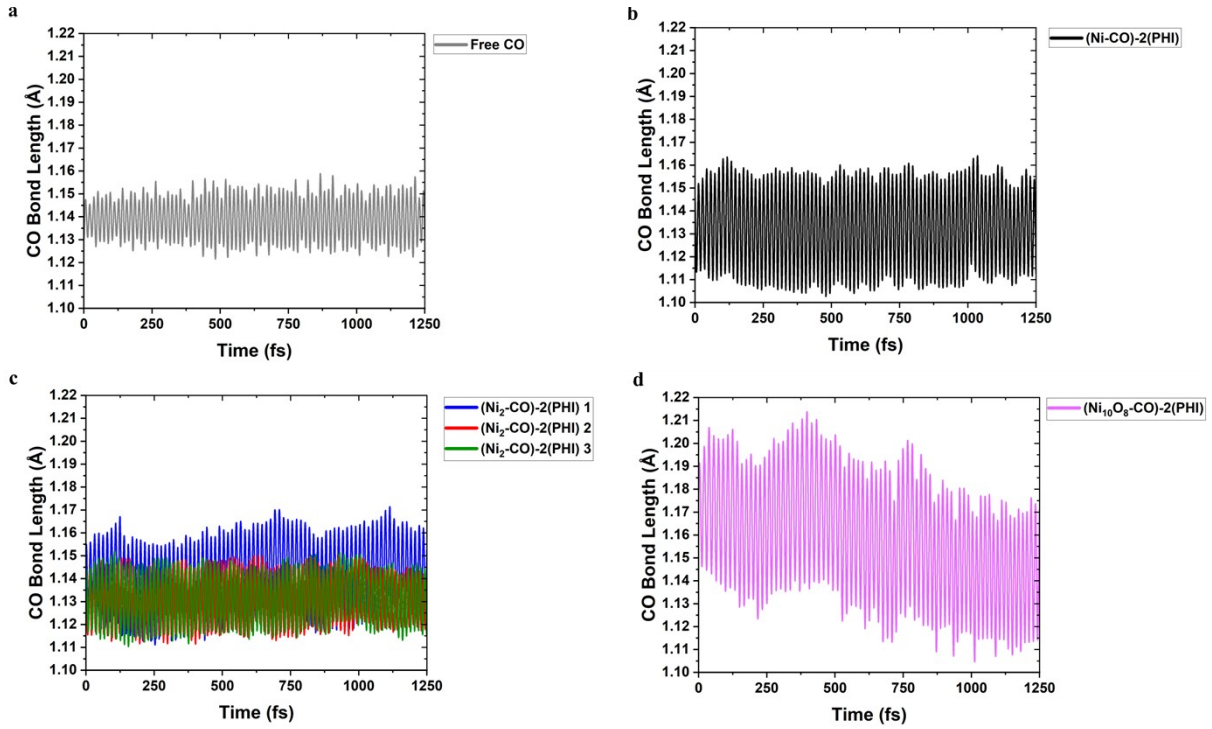

Figure S19. Time evolution of the CO bond length (Å) along 1.25 ps of each NVT DFT-MD equilibration for **a**, the free CO in grey line, **b**, the (Ni-CO)-2(PHI) system in black line, **c**, (Ni_2-CO)-2(PHI) systems **1**, **2**, and **3**, in blue, red, and green lines, respectively, and **d**, ($Ni_{10}O_8$-CO)-2(PHI) system in pink line.

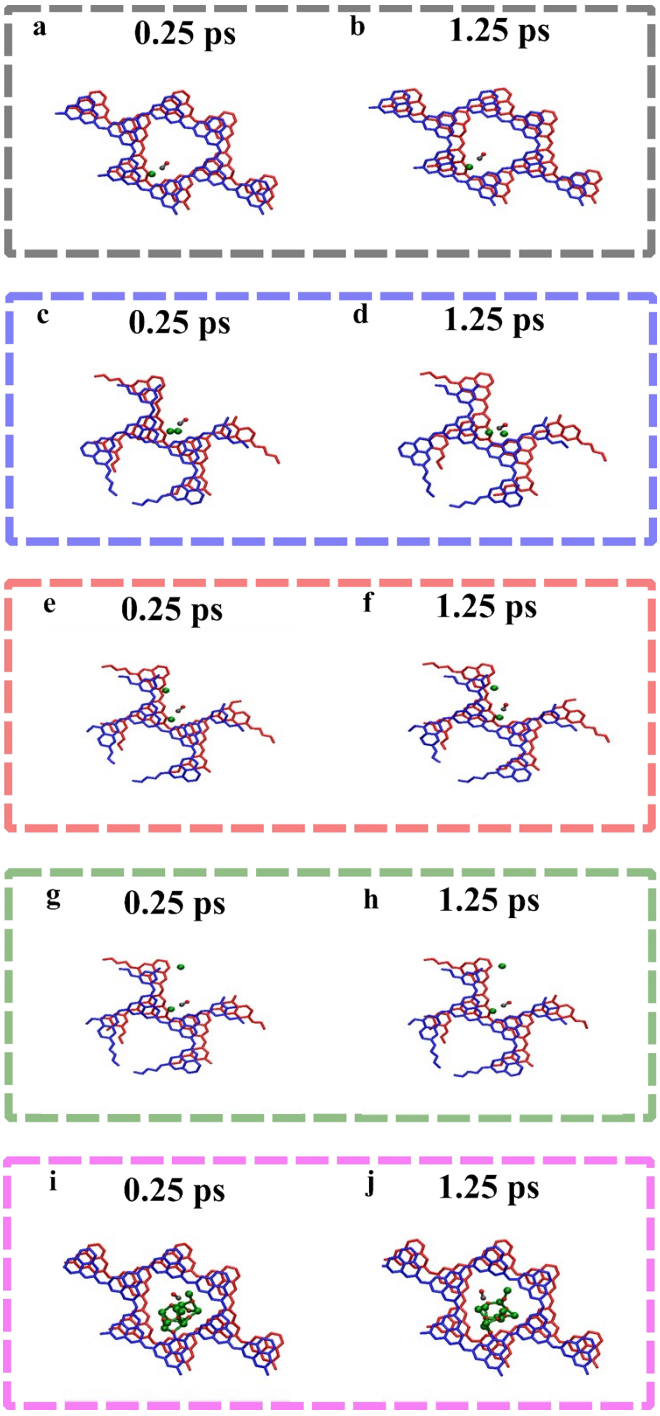

Figure S20. DFT-MD zoomed snapshots from top at 0.25 ps and 1.25 ps along the NVT MD trajectory, respectively, for **a**, and **b**, (Ni-CO)-2(PHI) system (black dash box), (Ni_2-CO)-2(PHI) **c**, and **d**, system **1** (blue dash box), **e**, and **f**, system **2** (red dash box), **g**, and **h**, system **3** (green dash box), and **i**, and **j**, ($Ni_{10}O_8$-CO)-2(PHI) (pink dash box), respectively. To highlight the PHI stacking shift, the top and bottom PHI layers are sketched as blue and red sticks, respectively. The nickel, carbon, and oxygen of the CO are depicted as green, grey, and red ball and stick, respectively. The Na^+ ions are omitted for clarity of the PHI stacking.

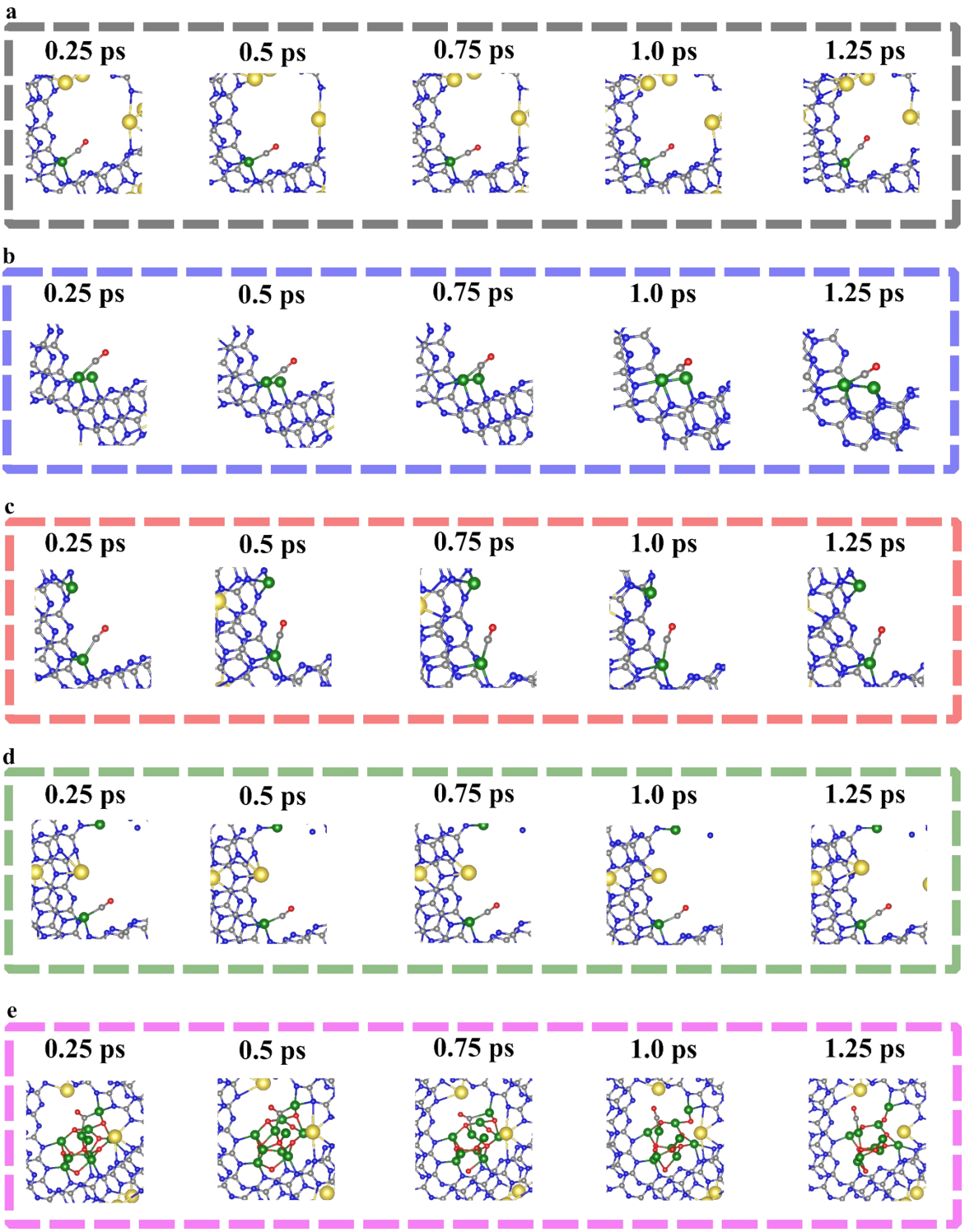

Figure S21. DFT-based MD zoomed snapshots at 0.25 ps, 0.5 ps, 0.75 ps, 1.0 ps, and 1.25 ps along the NVT DFT-MD trajectory, respectively, where the Ni-C_{CO} bond visualization cutoff is 2.3 Å, for **a**, (Ni-CO)-2(PHI) system (black dash box), (Ni_2-CO)-2(PHI) **b**, system **1** (blue dash box), **c**, system **2** (red dash box), **d**, system **3** (green dash box), and **e**, ($Ni_{10}O_8$-CO)-2(PHI) (pink dash box), respectively. The atoms are depicted as ball-and-stick models, with nickel in green, carbon in grey, nitrogen in blue, oxygen in red, and sodium in yellow.

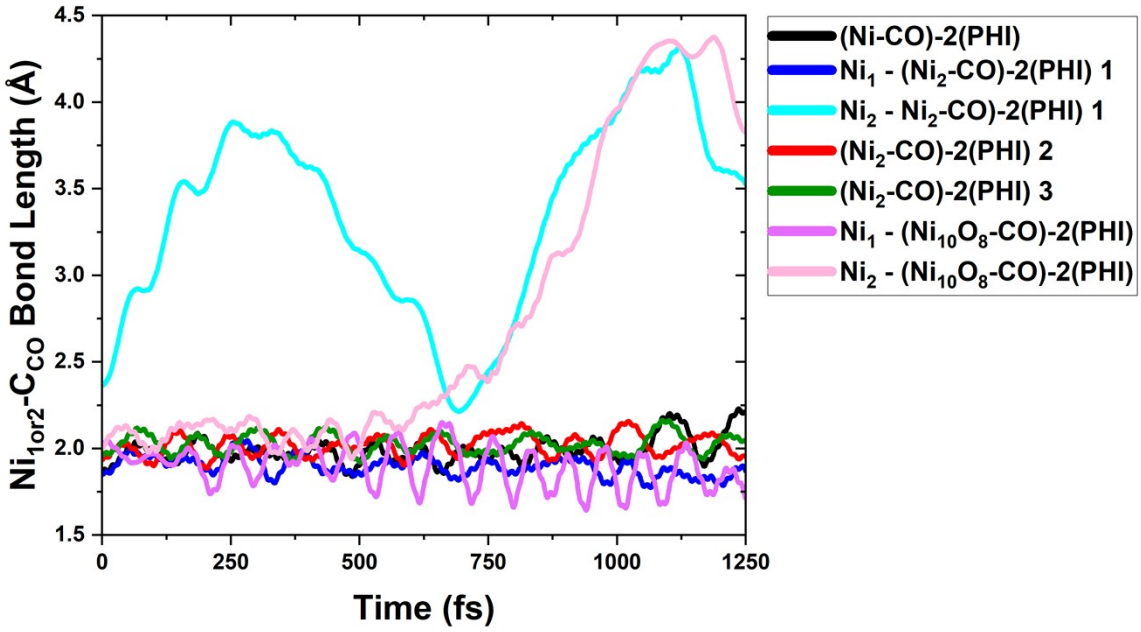

Figure S22. Time evolution of the Ni_{1or2}-C_{CO} bond length (Å) along 1.25 ps of each NVT DFT-MD equilibration for the (Ni-CO)-2(PHI) system (black line), and (Ni_2-CO)-2(PHI) systems **1** (blue and cyan lines), **2** (red line), and **3** (green line), and ($Ni_{10}O_8$-CO)-2(PHI) system (pink and light-pink lines).

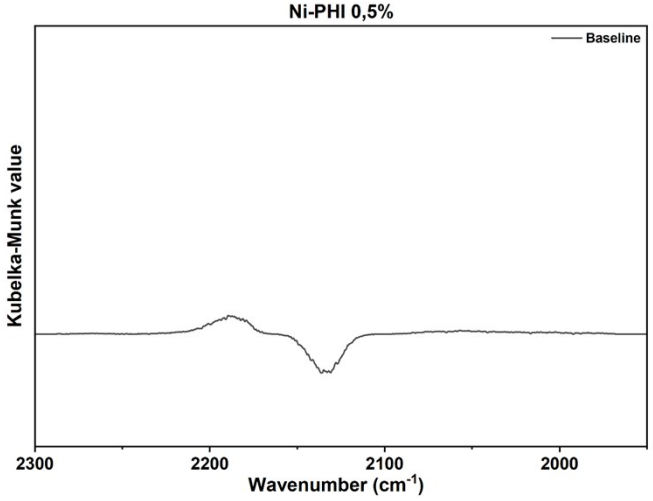

Figure S23. Example of baseline recorded under He after pretreatment (300 °C, 10 min) for *in situ* CO-DRIFTS spectra for Ni–PHI (0.5% Ni).

References

(1) Ye, H.-Z.; Berkelbach, T. C. Adsorption and Vibrational Spectroscopy of CO on the Surface of MgO from Periodic Local Coupled-Cluster Theory. *Faraday Discuss.* **2024**, *254*, 628–640. https://doi.org/10.1039/D4FD00041B.

(2) Tkalych, A. J.; Yu, K.; Carter, E. A. Structural and Electronic Features of β-$Ni(OH)_2$ and β-NiOOH from First Principles. *J. Phys. Chem. C* **2015**, *119* (43), 24315–24322. https://doi.org/10.1021/acs.jpcc.5b08481.